Impacts of Climate Change on the Food-Water Nexus in the Desert Southwestern U.S.

Xin Guan

School of Sustainable Engineering and the Built Environment, Arizona State University, Tempe, AZ, USA

Abstract

Quantifying the impacts of climate change on crop production is key to support integrated policies for the management of the food-energy-water (FEW) nexus. This is especially true in the water-limited desert southwestern U.S. Here, we applied the Water Evaluation and Planning (WEAP) platform and its crop model MABIA to simulate crop production in the main irrigation districts near Phoenix, Arizona, under different levels of warming and water allocations for irrigation. We first tested the ability of WEAP-MABIA to simulate water deliveries to all demand sectors and production of 11 crops during 2008–2018. In parallel, we evaluated and ranked the performances of 17 (10) general circulation models (GCMs) from CMIP5 (CMIP6) in reproducing the local climatology of eight variables needed to apply the crop model, finding no significant improvement of CMIP6 models. We then forced WEAP-MABIA with bias corrected and spatially interpolated GCM outputs under future warming scenarios. If current water allocations for irrigation are not varied, crop production is projected to decline with rates that are higher up to 2060 and reduced afterwards (constant rates up to 2100) under moderate (intense) warming scenarios. The decline rates vary with crop and scenario up to an ensemble mean of -4.8% per decade and are largely controlled by the simulated increase of potential and actual evapotranspiration. The effect of climate change is expected to become relatively less important if water shortages will exceed 10% of current allocations, which could possibly occur under the recently approved Colorado River Drought Contingency Plan. This work provides insights into (1) the utility of GCM outputs and water management models for crop simulations, and (2) future changes of the food-water nexus in southwestern U.S. that are needed to develop integrated FEW policies in the region.

1. Introduction

Irrigated agriculture plays a key role in the food-energy-water (FEW) nexus. This is especially true in hot and dry regions like the southwestern U.S. where agriculture is the largest water user under limited supply, mainly provided by energy intensive diversion transfers and groundwater (Yates et al., 2013). The future of agriculture in this region is challenged by population growth, development of other industries, and drought intensification due to global warming that could trigger water shortages (Cook et al., 2007; Fawcett et al., 2011; MacDonald, 2010; MacDonald et al., 2008). For example, Elias et al. (2016) reported that crop yields (i.e., crop production per unit of cultivated land) in southwestern U.S. have declined since 1978 on 11-21% of the total irrigated land, mostly because of surface water shortages and, to a minor extent, power shortages. While the need of integrated policies has been highlighted to promote synergies among the FEW sectors (Leck et al., 2015; Ringler et al., 2013), decisions are still made in insolation (Jones and White, 2021) with the potential unintended consequence of undermining local food security (MacDonald, 2010).

A key step to improve our understanding of FEW interactions and inform the development of integrated policies is to quantify crop productivity under global warming. Climate impacts agriculture in multiple and sometimes opposite ways. For example, higher CO_2 concentrations are expected to enhance crop yield (Tubiello et al., 2002); however, empirical studies indicate that this benefit will be counterbalanced when temperature increases above 30 ºC (Schlenker and Roberts, 2009; Wing et al., 2015). These conditions could be likely met for extended periods in southwestern U.S., where temperature is projected to rise by as high as 5 °C at the end of the century (Vose et al., 2017). Moreover, projected declines in snowpack (Easterling et al., 2017) and intensification of droughts (Seager et al.,

2007) will cause the probable reduction of streamflow in the Colorado River (Udall and Overpeck, 2017), which is the primary source of surface water in the region, thus triggering irrigation water shortages (USBR, 2021). While these arguments point to a decrease in crop production, estimates at smaller scales (e.g., irrigation districts) are more uncertain because they depend on local climate, soil conditions, and amounts of water cuts for irrigation (Reidmiller et al., 2018; Steele et al., 2018).

Estimates of crop production at local scales could be obtained by applying crop models that simulate the physiological processes of plant growth, seed formation, and yield along with soil water dynamics under different soil and weather conditions (e.g., Jabloun and Sahli, 2012; Jones et al., 2003; Keating et al., 2003). Crop models with diverse levels of sophistication have been applied at several sites and over various spatial extents to simulate changes in crop production using climate model outputs as forcings (e.g., Corbeels et al., 2018; Fraga et al., 2020; Osborne et al., 2013; Sommer et al., 2013; Wang et al., 2021; among many others). A review by White et al. (2011) of 221 studies of this type reported that most applications have (1) used only one or a few climate models, thus limiting the ability to quantify climate model uncertainty; (2) not accounted for the scale gap between the coarse grid spacing of climate model outputs and the field scale at which crop models are usually designed; (3) utilized mainly temperature and precipitation, neglecting other variables; and (4) incorporated changes in climate variables by adjusting historic data. While progress has been made, these issues are still largely present in more recent efforts (Peng et al., 2020) thus suggesting that research is needed to better incorporate climate model outputs into crop simulations.

The main goal of this study is to estimate crop production at the irrigation district scale in southwestern U.S. under different levels of warming and water allocations for irrigation. We focus on the main irrigation districts (IDs) near the Phoenix metropolitan region in central Arizona, which represents a compelling case study to investigate the future of the food-water nexus in desert southwestern U.S. In this urban region, agriculture was the main driver of the local economy up to World War II, but its importance has gradually diminished, as cropland has been converted into urban land to sustain one of the largest population growth in the country (Bausch et al., 2015; Fan et al., 2017). The region relies on limited water sources, including Colorado River water transported in a 541-km-long canal by the Central Arizona Project (CAP), which will most likely be subject to a shortage of 500,000 acre-feet (or 617 million m^3) in 2022-2023 affecting agricultural users in the state (USBR, 2021). Despite these challenges, agriculture is still a major water user and plays an important role in the regional economy (Duval et al., 2018). As a result, there is vivid interest on how agriculture could be sustained in the future and whether it should transition from a system focused on commodity crops, such as cotton and alfalfa that are mainly exported, to other configurations promoting local food security (Bausch et al., 2015).

To address our main goal, we built on our previous modeling effort of the FEW interactions in the Phoenix metropolitan region by Guan et al. (2020), who applied the Water Evaluation and Planning (WEAP) platform (Yates et al., 2005) to simulate annual water allocations to the main users under different FEW scenarios, while preserving water management rules and infrastructure constraints. Here, we expanded the calibration of WEAP focusing on the food-water nexus by (1) increasing the temporal resolution to monthly, (2) explicitly modeling water allocations to the main 12 IDs, and (3) using the embedded MABIA crop model (Jabloun and Sahli, 2012) to simulate production and irrigation demand of the major 11 crops. We tested the integrated model against estimates of water allocations from the Arizona Department of Water Resources (ADWR, 2021a) and of crop production from the U.S. Department of Agriculture (USDA, 2021a) in 2008-2018. We then explored the impacts of climate change by forcing the integrated model with daily outputs of 17 and 10 general circulation models (GCMs) from the Coupled Model Intercomparison Project Phase 5 (CMIP5) and Phase 6 (CMIP6), respectively, under scenarios of moderate and intense warming. We accounted for GCM errors by bias correcting and spatially interpolating the outputs. We first quantified potential variations of crop production that are only due to changes in climate forcings; this implied assuming unvaried water allocations for irrigation. We then evaluated changes under plausible water shortages following indications of the recent Colorado River Drought Contingency Plans (USBR, 2021). In all cases, we assumed no changes in cultivated area, crop types, and planting dates.

Our work provides novel methodological and practical insights on the impacts of climate change on the food-water nexus. Previous studies have tested performances of crop models using inputs from observed weather data. Here, we evaluated the crop model also when forced by historical climate model simulations, which is crucial to gain confidence on the reliability of future projections derived from the GCMs. To adequately characterize the model uncertainty, we used a large number of GCMs including those from the newest CMIP6 that we compared with the previous versions in CMIP5, a task that has just started to be addressed (e.g., Müller et al., 2021). We increased the GCMs' utility by evaluating several bias correction tools for a large number of variables needed to apply crop models, including precipitation, temperature, relative humidity, solar radiation and wind speed. This complements recent studies on the utility of bias correction of precipitation and temperature for crop modeling (Laux et al., 2021). Prior to applying the bias correction, we quantified the relative performances of the GCMs in reproducing the climatology of several variables, which is useful to support different types of impact studies in the region. Finally, our work is one of the few (e.g., Esteve et al., 2015) that integrated a water management and a crop model, so that reliable estimates of irrigated water could be obtained at the ID scale. To our knowledge, this work is also the first that quantifies changes in the food-water nexus at the metropolitan scale in southwestern U.S. Along with our recent studies of the water-energy nexus (Mounir et al., 2021, 2019), this work supports the development of regional integrated FEW policies.

2. Study Area

Our study domain is the Phoenix Active Management Area (AMA; Fig. 1), which is a political/hydrogeological region of ~14,600 km^2 created in 1980 by the Arizona Department of Water Resources (ADWR) with the primary purpose of achieving groundwater safe yield by 2025 (Higdon and Thompson, 1980). It is located in central Arizona (mainly in Maricopa County) and fully includes the Phoenix metropolitan area and its surrounding crop fields. Climate of this region is dry and warm all year round because of the quasi-permanent presence of a subtropical high-pressure ridge (Sheppard et al., 2002). The mean annual precipitation and temperature are 203 mm and 22 ºC, respectively, as observed at the Phoenix Encanto station (Fig. 1) of the Arizona Meteorological Network (AZMET) network in 1989-2019. For reference, Fig. 2 presents the climatological monthly means of several variables observed at this station. The precipitation regime includes two main seasons (Fig. 2a), including the North American Monsoon (NAM; Adams and Comrie, 1997) from July to September and a winter season from November to March. Details on the hydroclimatology of this region can be found in Mascaro (2017). Due to high temperature and low relative humidity, the atmospheric evaporative demand always exceeds precipitation in each month (Fig. 2). As a result, agriculture in this region relies almost entirely on irrigation, which mostly occurs between April and August when evapotranspiration is the highest (French et al., 2018).

Four main sources supply water to the municipal, agricultural, Native American, power and industrial users in the region: surface water from the Salt and Verde River basins managed by the Salt River Project (SRP; Phillips et al., 2009), surface water from the Colorado River delivered through the CAP canal, groundwater pumped from seven sub-basins in the AMA at about 27,500 wells (ADWR, 2021b), and reclaimed water. While the total volume supplied annually by the four sources remained fairly constant from 1985 to 2018 (~2800 million m^3), CAP water has been increasingly replacing GW to control overdraft (Higdon and Thompson, 1980).

Since Phoenix was established in 1881 and up to the end of World War II, agriculture was the only driver of the regional economy. After World War II, population started increasing and this stimulated the expansion of other industries, such as construction and later on high-tech companies. Over the last four decades, the rate of population growth was among the largest in the country, with the number of residents in the metropolitan area climbing from 1.85 million in 1985 to more than 4.95 million in 2019 (ADWR, 2021a; MAG, 2021). To sustain this growth in such a water-limited region, agricultural land has been gradually converted into urban land (Bausch et al., 2015; Fan et al., 2017; Kolankiewicz et al., 2020). According to ADWR (2021a), the irrigated cropland area decreased from roughly 1400 km^2 in 1985 to 630 km^2 in 2018 with a rate that stabilized since 2009. Despite this decrease, agriculture is still an important pillar of the regional economy. As of 2017, agriculture provides around 14,200 jobs (Duval et al., 2018), and sales of agricultural products contribute nearly $476 million to the economy of Maricopa County, which ranks 31st out of 3,073 counties in U.S. in this category (USDA, 2021b). According to USDA (2021a), the main crops cultivated in 2020 in the Phoenix AMA were alfalfa (64.6% of cropland area), cotton (8.1%), corn (7.5%), and winter wheat (4.1%).

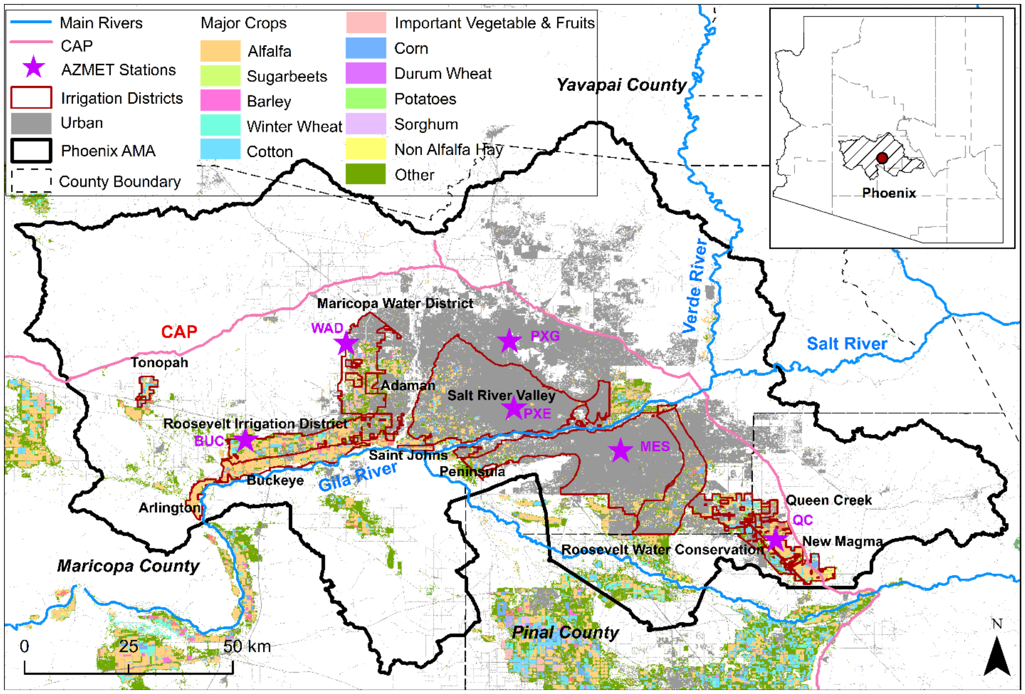

Figure 1. The Phoenix Active Management Area (AMA) in central Arizona, along with the 12 irrigation districts (Table 1); main crop types derived from the land cover map released by USDA (2021c) in 2017; six AZMET stations (codes reported in Table 2); the Salt, Verde, and Gila Rivers; and the Central Arizona Project (CAP) aqueduct.

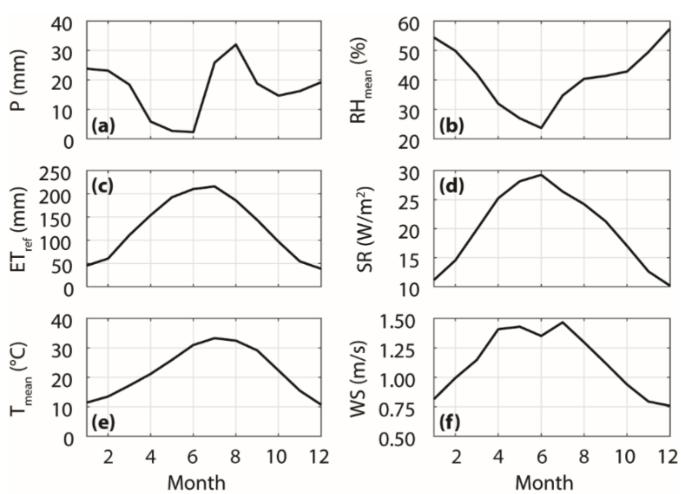

Figure 2. Climatological monthly mean of precipitation (P), reference evapotranspiration (ET_{ref}), mean temperature (T_{mean}), daily mean relative humidity (RH_{mean}), solar radiation (SR), and wind speed (WS) at the AZMET Phoenix Encanto Station over 1989-2019 (2003-2019 for ET_{ref}).

We identified 12 IDs in the region that use roughly 90% of irrigation water. Table 1 reports their name, mean cultivated area and top three crops over the period 2008–2018, mean elevation, and water portfolio. The cultivated area in each ID ranges from 1.84 km^2 to 100.38 km^2 (USDA, 2021c), with an average of 37.45 km^2. Alfalfa is the most important crop in all IDs; other major crops include fruit and vegetables, other (non-alfalfa) hay, winter wheat, corn, cotton, and oats. Depending on location and water rights, each ID relies on a different portfolio of water supply sources. All IDs use groundwater (from 3.2% to 93.8%); some of them receive water from CAP (up to 96.7%) and other surface water (up to 85.6%); and a few IDs use also a smaller fraction of reclaimed water (up to 1.6%).

3. Dataset

We set up and applied the WEAP-MABIA integrated model in 2008-2018 by integrating the data used in Guan et al. (2020; their Table 1) with new data sets that are introduced in Section 4.1.2 in the description of the model setup. We obtained daily precipitation (P); mean (T_{mean}), minimum (T_{min}), and maximum (T_{max}) air temperature at 1.5 m; mean (RH_{mean}) and minimum (RH_{min}) relative humidity; mean wind speed (WS) at 3 m; solar radiation (SR); and reference evapotranspiration (ET_{ref}) data recorded by six weather stations belonging to the AZMET network for variable periods from 1988 to 2019. Depending on their location and time availability, some of these stations were used to apply MABIA and others to bias correct and interpolate climate model outputs (Fig. 1; Table 2). We also obtained a 10-m digital elevation model (DEM) from the USGS 3D Elevation Program (USGS, 2021) and used it to spatially interpolate the bias-corrected climate model outputs.

We acquired daily outputs of 17 and 10 GCMs from CMIP5 and CMIP6, respectively, for the same variables mentioned for the AZMET stations. Climate model outputs and observed data of WS were converted to 2 m above ground based on Brown (2005). Table 3 reports, for each model, acronym, climate center, and grid horizontal spacing ranging from about 0.70° to 3.75°. We obtained outputs for the historical experiment and for future scenarios of moderate and intense warming, including RCP4.5 and RCP8.5 for CMIP5 (with RCP being the Representative Concentration Pathway; Van Vuuren et al., 2011), and the equivalent SSP2-4.5 and SSP5-8.5 for CMIP6 (with SSP being the Shared Socioeconomic Pathway; O'Neill et al., 2016). The historical experiment spans the period from 1950 to 2005 (2014) for CMIP5 (CMIP6), while the future scenarios range from 2006 (2015) to 2099 for CMIP5 (CMIP6). We acquired ensemble "r1i1p1" ("r1i1p1f1") for CMIP5 (CMIP6) for the climate variables, along with elevation grids required to apply the spatial interpolation routines. All outputs were downloaded from the Earth System Grid Federation (ESGF) repositories.

Irrigation District (ID)	**Cultivated area (km^2)**	**Main crops (% total)**		**Elevation (m)**	**Water Portfolio (%)**			
					CAP	**Ground water**	**Reclaimed Water**	**Surface Water**
Adaman	4.56	Alfalfa	30.5	335.6	0.0	61.5	0.0	38.5
		Potatoes	11.1					
		Corn	7.6					
Arlington	16.41	Alfalfa	73.7	236.6	0.0	14.4	0.0	85.6
		Sorghum	6.4					
		Other Hay/Non Alfalfa	4.9					
Buckeye	69.05	Alfalfa	74.5	260.4	0.0	24.0	0.0	76.0
		Barley	6.3					
		Cotton	5.0					
Maricopa Water District	33.00	Alfalfa	27.6	361.3	26.5	37.2	0.0	36.3
		Corn	12.5					
		Carrots	8.4					
New Magma	71.89	Alfalfa	59.4	464.4	96.7	3.2	0.0	0.0
		Cotton	18.7					
		Corn	5.1					
Peninsula	1.84	Alfalfa	81.7	303.6	0.0	21.5	0.0	78.5

		Corn	4.7					
		Cotton	4.2					
Queen Creek	28.68	Alfalfa	46.5	431.2	87.5	12.5	0.0	0.0
		Cotton	20.2					
		Corn	14.3					
Roosevelt Irrigation District	100.38	Alfalfa	49.0	289.3	2.3	93.8	1.1	2.8
		Cotton	20.1					
		Durum Wheat	11.3					
Roosevelt Water Conservation District	33.71	Alfalfa	69.7	392.7	75.0	12.3	1.6	11.1
		Corn	16.9					
		Winter Wheat	2.5					
Saint Johns	4.67	Alfalfa	74.9	287.0	0.1	66.3	0.0	33.5
		Cotton	6.5					
		Other Hay/Non Alfalfa	5.1					
Salt River Valley	71.54	Alfalfa	64.8	350.7	0.1	33.5	0.1	66.3
		Cotton	12.1					
		Corn	7.4					
Tonopah	13.61	Alfalfa	47.5	351.1	67.3	32.7	0.0	0.0
		Corn	19.9					
		Cotton	15.6					

Table 1. The 12 irrigation districts (IDs) consuming 90% of irrigation water in the Phoenix AMA. For each ID, name, mean cultivated area and three main crops in 2008–2018, mean elevation, and water portfolio are reported.

Station Name	Abbreviation	Latitude	Longitude	Elevation (m MSL)	Available period	Purpose of use
Citrus Farm / Waddell	WAD	33.62	-112.46	406.0	1988-2009	1
Phoenix Greenway	PXG	33.62	-112.11	403.0	1988-2019	1
Phoenix Encanto	PXE	33.48	-112.10	334.0	1989-2019	1, 2
Queen Creek	QC	33.19	-111.53	462.0	1996-2019	1, 2
Buckeye	BUC	33.41	-112.68	301.0	1999-2019	1, 2
Mesa	MES	33.39	-111.87	368.0	2004-2019	2

Table 2. AZMET stations used in this study, including abbreviation, location, elevation, and available period of observed records. Purpose of use 1 is to assess performance and bias correct climate model outputs. Purpose of use 2 is to apply WEAP-MABIA with observed data.

	Model Name	Modeling Center	Latitude grid spacing (degrees)	Longitude grid spacing (degrees)
CMIP5	ACCESS1-0	CSIRO-BOM	1.250	1.875
	ACCESS1-3		1.250	1.875
	CanESM2	CCCma	2.789	2.813
	CNRM-CM5	CNRM-CERFACS	1.400	1.406
	CSIRO-Mk3.6.0	CSIRO-QCCCE	1.865	1.875

	GFDL-CM3	NOAA GFDL	2.000	2.500
	GFDL-ESM2G		2.011	2.500
	GFDL-ESM2M		2.011	2.500
	HadGEM2-CC	MOHC	1.250	1.875
	HadGEM2-ES		1.250	1.875
	IPSL-CM5B-LR	IPSL	1.895	3.750
	IPSL-CM5A-LR		1.895	3.750
	IPSL-CM5A-MR		1.268	2.500
	MIROC5	MIROC	1.400	1.406
	MIROC-ESM		2.789	2.813
	MIROC-ESM-CHEM		2.789	2.813
	MRI-CGCM3	MRI	1.121	1.125
CMIP6	ACCESS-CM2	CSIRO-ARCCSS	1.250	1.875
	CanESM5	CCCma	2.789	2.813
	EC-Earth3	EC-EARTH	0.702	0.703
	GFDL-CM4	NOAA GFDL	1.000	1.250
	INM-CM4-8	INM	1.500	2.000
	INM-CM5-0		1.500	2.000
	IPSL-CM6A-LR	IPSL	1.268	2.500
	MPI-ESM1-2-HR	MPI-M	0.935	0.938
	MPI-ESM1-2-LR		1.865	1.875
	MRI-ESM2-0	MRI	1.121	1.125

Table 3. GCMs used in the study.

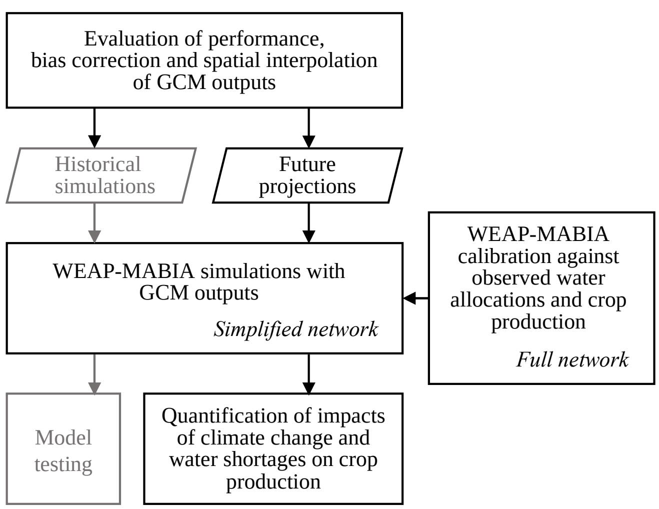

Figure 3. Schematic of the approach adopted to simulate the impact of climate change on crop production in the Phoenix AMA.

4. Methodology

Our methodological framework is summarized in the diagram of Fig. 3. We used WEAP-MABIA to simulate crop water demand and production in the study region. We first calibrated the model using observed inputs and, in parallel, we evaluated the GCMs ability to reproduce the climatology of all aforementioned climate variables observed by the AZMET stations. We then applied bias correction and spatial interpolation techniques to generate daily spatial maps at 500-m resolution for each variable in the historical and future periods. These fields were used to apply WEAP-MABIA first in the historical period to assess whether the use of bias-corrected GCM outputs allows capturing observed mean annual water allocations and crop production. After this was verified, we forced the calibrated WEAP-MABIA model with GCM future projections to explore the impact of climate change on crop production.

4.1 Brief description of WEAP-MABIA and its setup in the Phoenix AMA

4.1.1. Model description

WEAP is a water resource management model that simulates water fluxes in a network of supply sources and demand nodes connected by transmission links (Yates et al., 2005). This is done through an optimization routine constrained by mass balance, demand priorities, supply preferences, and infrastructure (e.g., canals, reservoirs) size and operating rules. Time-varying water supply fluxes from rivers and reservoirs are prescribed through time series or calculated internally by applying a rainfall-runoff model and reservoir management schemes. Aquifer physical properties are assigned to control groundwater extraction. Water demands are specified through external time series or computed as a function of annual activity levels (e.g., population) and water use rates (e.g., per-capita water demand), which are then distributed monthly based on prescribed fractions of the annual totals. WEAP outputs several variables quantifying fluxes and storages in all elements of the network.

To quantify the agricultural water demand, an alternative option is the use of the embedded MABIA module (Jabloun and Sahli, 2012), which also allows estimating crop yield. In the WEAP network, different agricultural demand nodes could be defined with a related crop portfolio. In each of these nodes, MABIA calculates the root-zone soil water balance at daily time scale, where the fluxes include effective precipitation, surface runoff, irrigation, actual crop evapotranspiration (ET_a), capillary rise from the groundwater table (if existing), and deep percolation. To estimate each term, it is necessary to provide daily climate variables as input, and assign soil and crop properties. Of particular importance is the estimation of ET_a as $ET_a = K_{act} \cdot ET_{ref}$, where ET_{ref} is the reference evapotranspiration and K_{act} is the actual crop coefficient. Time series of ET_{ref} are either provided as external forcings or calculated internally with the Penman-Monteith equation (Allen et al., 1998) using input climate variables. Estimates of ET_a are used to derive the crop yield as a function of crop-dependent parameters. Built-in libraries are available with crop parameters for hundreds of crops (Doorenbos and Kassam, 1979) and soil parameters for the main texture classes. Another important term of the root-zone soil water balance is irrigation, which is controlled by the irrigation efficiency, i.e., the fraction of the supplied water than can effectively reach the crop and be available for evapotranspiration (WEAP, 2020). This parameter varies among different irrigation types (Brouwer et al., 1989). MABIA does not account for the effect of CO_2 in the estimation of crop yield. Additional details on MABIA and its integration with WEAP are provided in the Supplementary Material, along with relevant references of model applications.

4.1.2 Model setup with observed data and verification with historical climate simulations

We delineated the water demand and supply network of the Phoenix AMA in the WEAP platform based on the configuration of Guan et al. (2020). In that study, the network consisted of four supply sources, including CAP, SRP, groundwater, and reclaimed water; and six demand nodes, including municipal, agricultural, Native American, industrial, power plants, and riparian. Here, as shown in Fig. 4a, we expanded the configuration of Guan et al. (2020) by disaggregating the agricultural demand node into 12 nodes representing the IDs of Table 1. Each ID was linked to specific water sources based on the corresponding water portfolio and the capacity of the transmission links was limited by the maximum percent of demand that can be satisfied by a given source, as reported in Table 1. We used the cropping patterns from USDA (2021c) to identify 11 crops accounting for nearly 98% of the cropland area of all 12 IDs over the period 2008–2018. These include alfalfa, barley, cotton, durum wheat, corn, sorghum, potato, sugarbeets, winter wheat, other (not alfalfa) hay, and vegetable and fruits (accounting for several crops combined in a single category). In each ID, we implemented all 11 crops and assigned the corresponding percentage of the total area, which could be zero when a crop was not cultivated in a given year. For each crop, we derived the parameters needed to solve the water balance and estimate yield from the MABIA crop library. We specified the soil parameters in each ID by extracting the main soil texture from USDA (2021d) and obtaining the associated soil parameters from the MABIA soil library. We then provided daily P, RH_{min}, WS, and ET_{ref} (calculated as described in Brown (2005)) from the closest AZMET stations (Table 2) as inputs for the computation of the water balance in each ID.

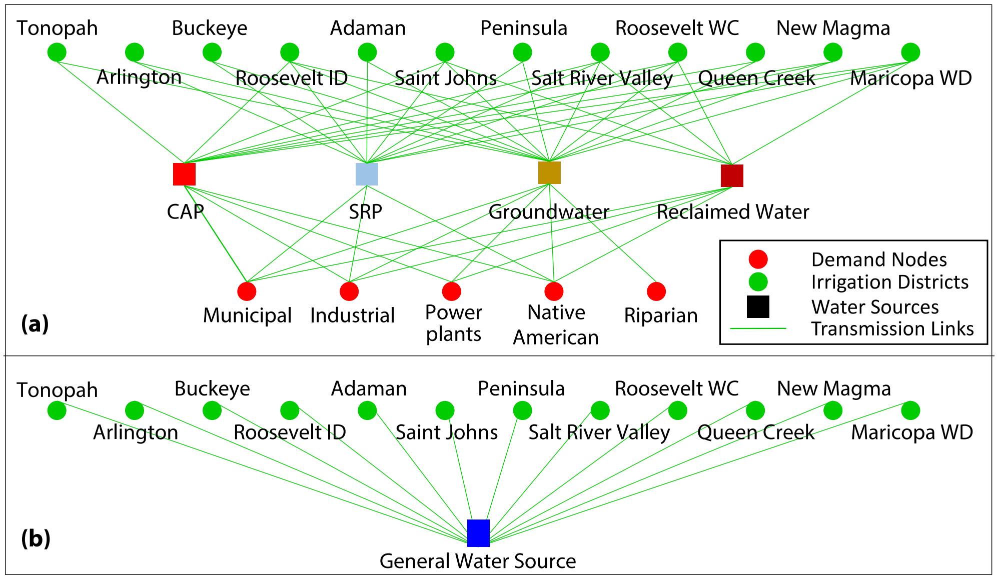

Figure 4. WEAP-MABIA model configurations in the Phoenix AMA with (a) full and (b) simplified networks.

For the other demand sectors, we obtained the annual demands from ADWR (2021a), similar to Guan et al. (2020). We then disaggregated the municipal (industrial and power plant) demand to monthly scale using mean monthly variations of residential (non-residential) water use reported by the City of Phoenix Water Service Department (2011). Due to lack of information, we assumed constant monthly demand for the Native American sector, which only accounts for 11.9% of the total annual demand. We prescribed water inflows from SRP and CAP from 2008 to 2018 using the same data sources and approach described in Guan et al. (2020; their Section 3.3 and Supporting Information), and further increased the temporal resolution to monthly using data from SRP (2021) and CAP (2021), respectively. We calibrated WEAP-MABIA using observed climate data in the period 2008–2018 as inputs. We started from an irrigation efficiency of 0.6 at all IDs as suggested by FAO (Brouwer et al., 1989) for furrow irrigation, which is the most common practice in the region, and changed this value to 0.65 to match estimates of water use from ADWR (2021a) and crop production from USDA (2021a).

4.1.3 Model setup and simulations under future climate projections

To investigate the impacts of climate change, we applied WEAP-MABIA with a simplified network configuration containing the 12 IDs as demand nodes and a single water supply node combining all sources (Fig. 4b). This network was designed to quantify the impacts on crop production due solely to future changes in climate variables and prescribed reductions of water allocations for irrigation, without making subjective assumptions on future trends of water demand from the other sectors and supply sources that are out of the scope of this paper. The model was set up and parameterized using information from the calibrated model of Fig. 4a. For each ID: (1) the maximum capacity of the transmission link with the general water source was set equal to the mean total water allocations from all sources simulated by the calibrated model in 2008–2018; this capacity was varied each month and reduced for simulations with prescribed irrigation water shortages; (2) a constant area was assumed for each crop type, computed as the mean area across 2008–2018; and (3) the same parameters for MABIA, including irrigation efficiency, were adopted from the calibrated model. For the general water source, while we did not assume any limitation in water availability, this was implicitly introduced by fixing the maximum capacities of the transmission links with the IDs. Simulations were conducted by forcing MABIA with bias corrected GCM outputs for the historical period and future projections. We tested the reliability of this simplified configuration by comparing the mean observed annual water allocations and crop production with simulations under historical climate model forcings.

4.2 Performance evaluation, bias correction, and spatial interpolation of climate models

We first evaluated the GCMs' ability to capture the monthly climatologies of all variables, as observed by five AZMET stations with more than 20 years of records (Table 2). For each station and GCM, we found the co-located climate model pixel and calculated time series of monthly mean (or total for P) values for each variable. This was done for the same number of years used to derive the temporal means from the AZMET records. Since the AZMET records extend beyond the end of the GCM historical simulations, we selected the closest period with the same number of years. For example, for the PXE station, observations are available from 1989-2019; we then processed GCM outputs from the closest period of 31 years from 1975 to 2005 (1984 to 2014) for CMIP5 (CMIP6). We quantified differences between observed and simulated time series by computing correlation coefficient (CC), normalized root-mean-square difference (CRMSD, as defined in Equation 1), and temporal standard deviation (STD) – which were used in the Taylor diagram (Taylor, 2001) – and bias (B, as defined in Equation 2). We then ranked the climate models based on their performances in reproducing the seasonality of both individual and all climate variables, by using the dimensionless relative error metric of Deidda et al. (2013) that combines CRMSD, STD, and CC.

$$CRMSD = \left\{\frac{1}{12}\sum_{m=1}^{12}\left[\left(x_{SIM,m} - \bar{x}_{SIM}\right) - \left(x_{REF,m} - \bar{x}_{REF}\right)\right]^2\right\}^{1/2} \quad (1)$$

$$B = x_{SIM,m} - x_{REF,m} \quad (2)$$

where $x_{SIM,m}$ and $x_{REF,m}$ are the climatological means of a given variable x simulated by a GCM and provided by a reference dataset (here, an AZMET weather station), respectively, in month $m = 1, \ldots, 12$; and $\bar{x}_{SIM}$ ($\bar{x}_{REF}$) is the mean value of $x_{SIM,m}$ ($x_{REF,m}$). The standard deviation (STD) across the 12 months is calculated for $x_{SIM,m}$ ($\mathrm{STD_{SIM}}$) and $x_{REF,m}$ ($\mathrm{STD_{REF}}$). We used the normalized Taylor diagram, where $\mathrm{STD_{REF}}$ and $\mathrm{STD_{SIM}}$ are divided by $\mathrm{STD_{REF}}$.

We bias corrected daily GCM outputs using each of the five selected AZMET stations as reference. Previous studies (e.g., Teutschbein and Seibert, 2012) suggested that techniques based on quantile mapping (Boé et al., 2007) allow correcting a larger number of statistical properties of the variables compared to simpler methods, such as linear scaling, variance scaling, and delta change. We then tested first parametric quantile mapping methods, by evaluating the goodness-of-fit via the Lilliefors test of several distributions (e.g., Gaussian, gamma, and beta) to capture the quasi symmetric (T_{mean}, T_{min}, and T_{max}), positively (P, WS) and negatively (SR) skewed, and bounded (RH_{mean} and RH_{min}) empirical distributions of the climate variables. Unfortunately, we did not find any adequate distribution for all variables except for P. For this variable, we adopted the parametric method of Mamalakis et al. (2017). For the other variables, we considered the quantile mapping bias correction based on the empirical distributions. This technique has the drawback that assumptions should be made on the frequency of future values located outside of the interval of the distribution of the historical simulations. This happens only on less than 5% of the cases for RH_{mean}, RH_{min}, WS, and SR, so that the empirical quantile mapping was used for these variables. For T_{mean}, T_{min}, and T_{max}, the number of future values outside of the historical simulations' range is larger and the alternative variance scaling method proposed by Chen et al. (2011) was used. The bias correction of all variables except P was applied month by month. For P, it was performed for winter (November–March), spring (April–June), and each of the summer monsoon months (July–October) to retain a sufficient number of nonzero precipitation values.

After bias correcting the GCM outputs at the five locations of the AZMET stations, we spatially interpolated the variables in a 500-m grid covering the Phoenix AMA. For all variables except P, we applied the techniques of Liston and Elder (2006) that are based on the Barnes objective analysis scheme

(Barnes, 1994; Koch et al., 1983) and terrain information. We generated terrain, slope, and curvature grids at 500-m resolution using the DEM from USGS (2021) and used elevation to interpolate T_{mean}, T_{min}, T_{max}, RH_{mean}, RH_{min}; slope for SR; and slope and curvature for WS. We tested the performance of the interpolation method through leave-one-out cross validation, namely: (i) we left out one of the stations and applied the method using the remaining four stations; (ii) we compared interpolated and observed time series of all variables at the left-out station; and (iii) we repeated (i)-(ii) for all stations. The comparison was done by computing relative root mean square error (RRMSE), CC, and relative bias (RB) (RRMSE and RB are defined in Equation 3 and 4). For P, we applied the nearest neighbor interpolation method. Once the 500-m daily grids were generated for the historical and future periods, the spatial means of all variables were extracted in each ID and used as climatic inputs for WEAP-MABIA.

$$RMSE = \frac{\sqrt{\frac{1}{12}\sum_{m=1}^{12}\left(x_{SIM,m}-x_{REF,m}\right)^2}}{\frac{1}{12}\sum_{m=1}^{12}x_{REF,m}} \times 100 \tag{3}$$

$$RB = \frac{\frac{1}{12}\sum_{m=1}^{12}(x_{SIM,m}-x_{REF,m})}{\frac{1}{12}\sum_{m=1}^{12}x_{REF,m}} \times 100 \tag{4}$$

where $x_{SIM,m}$ and $x_{REF,m}$ are the climatological means of a given variable *x* simulated by the spatial interpolation method and provided by a reference dataset at one left-out AZMET station in month m = 1, …, 12, respectively.

5. Results

We first present results of climate model performance evaluation and bias correction, and then illustrate the outcomes of the simulations with WEAP-MABIA.

5.1 Climate model performance in the historical period

GCM performances are summarized in Figs. 5 and 6, which present the normalized temporal Taylor diagram and the monthly bias, respectively, for representative variables using one of the AZMET stations as reference (results for other variables are shown in Fig. S1, while they are not reported for other reference stations because they are conceptually similar). We first note that all models have very good ability to capture amplitude and phasing of the annual cycle for T_{mean} and SR (see Taylor diagrams of Fig. S1). This capability is still fairly good for RH_{mean} (CC > 0.6; Figs. 5a,b), although the variability tends to be larger (STD up to 2.1 times the observation). The GCMs have less skill at capturing the seasonality of P (CC mainly between 0.20 and 0.60; Figs. 5c,d), which is simulated with larger amplitudes and errors (STD and CRMSD up to 4 times the observed STD). The models represent the seasonality of WS with a large range of accuracy ($-0.83 \leq CC \leq 0.98$; Figs. 5e,f), but all capture the amplitude relatively well (STD and CRMSD up to 2.6 times the observed STD).

Turning now our attention to the bias (B), Fig. 6 shows that most GCMs underestimate T_{mean} with negative B up to -9.6 °C, while the opposite is true for SR, especially in summer when B reaches +4.2 MJ/m^2. RH_{mean} exhibits seasonal B, with positive values in winter (up to 32%) and negative in summer (up to -22%). These trends are similar for P, given the relation between these two variables, with B being as high as +3.2 mm/day (as low as 0.9 mm/day) in winter (summer). The models from GFDL and IPSL centers have positive B for RH_{mean} and P also in late summer and fall. Finally, WS is largely overestimated by the GCMs, especially during the winter season when B reaches +3.2 m/s.

5.2 Bias correction and spatial interpolation of GCM outputs

Examples of results of the selected bias correction methods are shown in Fig. 7, where quantile-quantile (Q-Q) plots are presented between observed and simulated empirical distributions of representative variables for the CanESM2 model, chosen as example. The observed distribution is perfectly captured for WS and RH_{mean} when using the nonparametric bias correction, and quite well reproduced for P (including the largest quantiles) through the parametric method of Mamalakis et al. (2017). The simpler variance scale bias correction method allows also representing well the observed distribution of T_{mean}, although with a slight overestimation of the lower quantiles. Results are substantially similar for other variables, months, and models.

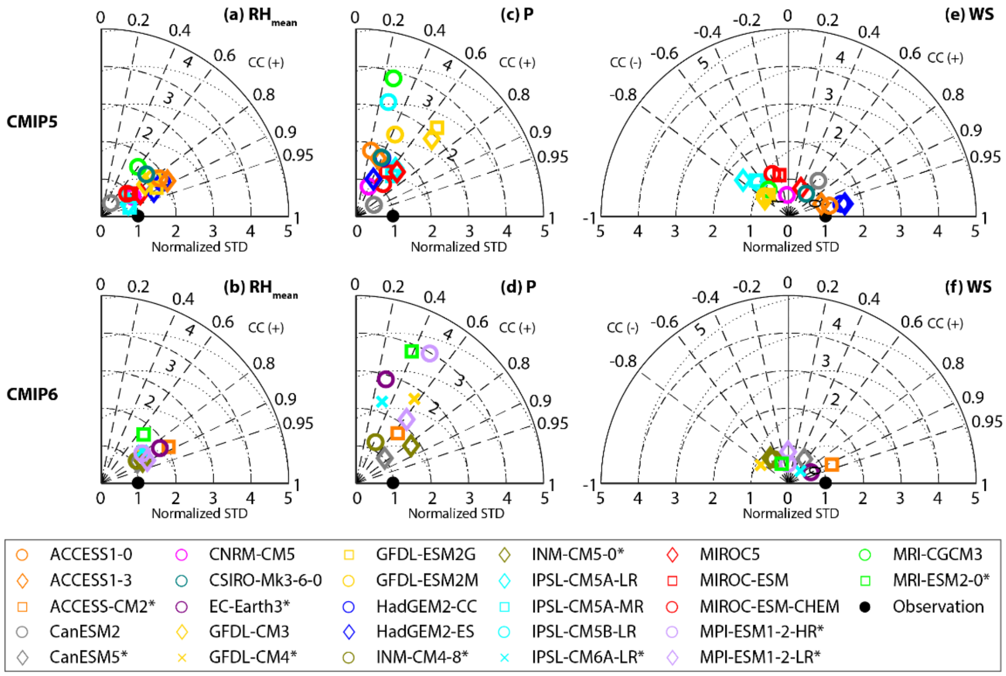

Figure 5. Normalized temporal Taylor diagram for (a)-(b) RH, (c)-(d) P and (e)-(f) WS computed using PXE station as reference. Top (bottom) panels are referred to CMIP5 (CMIP6) models. In the Taylor diagrams, the black circle is the observed value where the normalized STD = 1, the radial distance from the black circle is the normalized CRMSD, the azimuth and the radial distance from the origin are CC and normalized STD, respectively. In the legend, GCMs are displayed with the same color if belonging to the same modeling center.

As a next step, we interpolated the bias corrected variables at the five weather stations (Table 2) into a 500-m resolution grid following Liston and Elder (2006). This was done for all variables except for P. Fig. 8 shows examples of this process for T_{mean} and WS in one day, including the original variables in the coarse grid of one of the GCMs; high-resolution terrain features used for the spatial interpolation; and bias corrected variables in the high-resolution grid. The overall bias correction and spatial interpolation procedure was tested through leave-one-out cross validation. Results are summarized in Figs. 9a-c through heat maps of metrics quantifying the ability to capture the monthly climatology of the left-out station. The method works quite well for all variables and locations (averaged CC ~ 1.00, RRMSE = 5.0%, and RB = -0.05%), with the exception of WS at BUC, QC, and WAD stations (lowest CC = 0.64; largest RRMSE = 44.3% and RB = -43.0%). The simulated and observed monthly climatologies for three representative variables and sites are presented in Figs. 9d-f for reference.

5.3 Simulation of crop production and irrigation requirements in the historical period

Performances of the calibrated WEAP-MABIA model applied with the full network of Fig. 4a and observed climate forcings are summarized in Fig. 10. The model simulates quite well the annual water allocations from the different sources to the agricultural and all other demand sectors estimated by ADWR (Figs. 10a-d), as well as the production of the main crops obtained from USDA (Figs. 10e-h). The calibrated model was then applied with bias corrected and spatially interpolated GCM outputs in the historical period with the simplified configuration of Fig. 4b. To evaluate performances, we computed the ratio between simulated and observed climatological means of annual water allocations to all IDs and of crop production. As shown in Fig. 11, simulations with all GCMs capture remarkably well water allocations to all IDs, as shown by the ratio (labeled relative mean) being practically 1 in all cases. The mean crop production is also reproduced well, especially for alfalfa (the crop with the largest production). For some crops, production is moderately overestimated (barley) or underestimated (cotton and durum

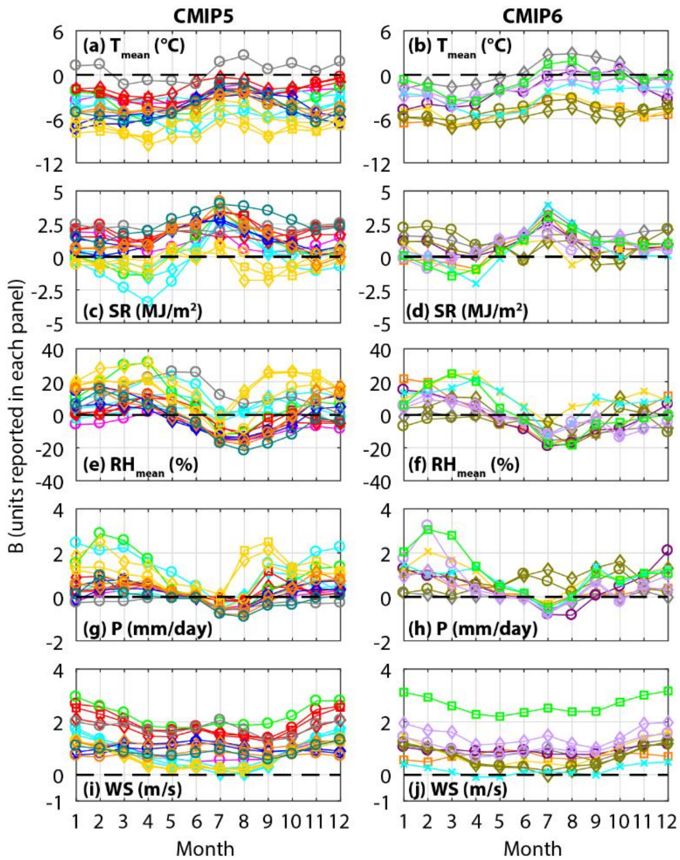

Figure 6. Monthly bias (B) for T_{mean}, SR, RH_{mean}, P and WS computed using PXE station as reference. Left (right) panels show results for CMIP5 (CMIP6) GCMs. The legend is reported in Fig. 5.

wheat). This outcome is not due to errors in climate forcings but to the assumption made for the simplified configuration of a constant cultivated area (equal to the temporal mean), which instead fluctuated in 2008-2018 for these crops. Such explanation is confirmed by the fact that simulations with observed climate data from AZMET are always consistent with results for the GCMs. Overall, these findings indicate that our framework combining bias corrected GCMs and WEAP-MABIA allows historic crop production and irrigation requirements to be reliable simulated in the study region, thus providing confidence on its use under future forcings.

5.4 Future projections of climate variables and crop production

We first present changes of the main climate variables in the two future scenarios, evaluated as anomalies of bias corrected values relative to the mean over the last 11 years of the historical simulation (1995-2005 for CMIP5; 2004-2014 for CMIP6). This reference period was selected to be as consistent as possible with duration and time period of the calibrated crop simulations. To characterize the uncertainty across the climate models, we used the method of Sanderson et al. (2017) to compute ensemble mean and 90% confidence intervals (CIs) as weighted averages accounting for (i) potential interdependencies across GCMs due to similarities in model parameterizations, and (ii) GCMs' skills in simulating local climatological characteristics. Fig. 12 shows the 11-year moving average of the anomalies spatially averaged over the Phoenix AMA, along with the 90% CI across climate models. We first note that, for all variables, the uncertainty quantified through the width of the 90% CIs increases with time. GCMs predict very little variations of annual P in both future scenarios. T_{mean} is projected to steadily increase by an ensemble mean of nearly 2.7 ºC (5.4 ºC) by the end of the century for RCP45 and SSP245 (RCP85 and SSP585) scenarios. RH_{mean} is instead predicted to decline by 2.7% to 3.6%, particularly under the intense warming scenarios, as also found in previous studies that ascribed this outcome to the possible effect of faster warming on land compared with the oceans (O'Gorman and Muller, 2010; Sherwood and Fu, 2014; Simmons et al., 2010). WS and SR do not show a significant difference between historical and future periods, with the exception of a slight decrease of SR (about -0.2 MJ/m^2 or -1%) projected after 2080 for the RCP85 and SSP585 scenarios. Such a change could be due to the combined effect of aerosol loading,

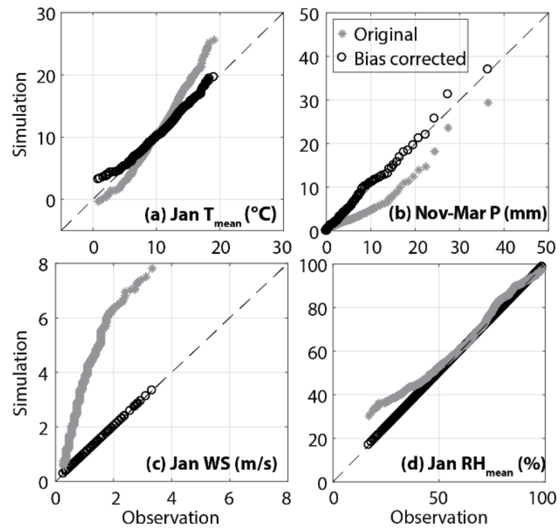

Figure 7. Q-Q plot between (i) the observed distributions of daily T_{mean}, WS, and RH_{mean} in January and P in winter (November-March) at the PXE station, and (ii) the original and bias corrected distributions of historical simulations with CanESM2 in the co-located pixel.

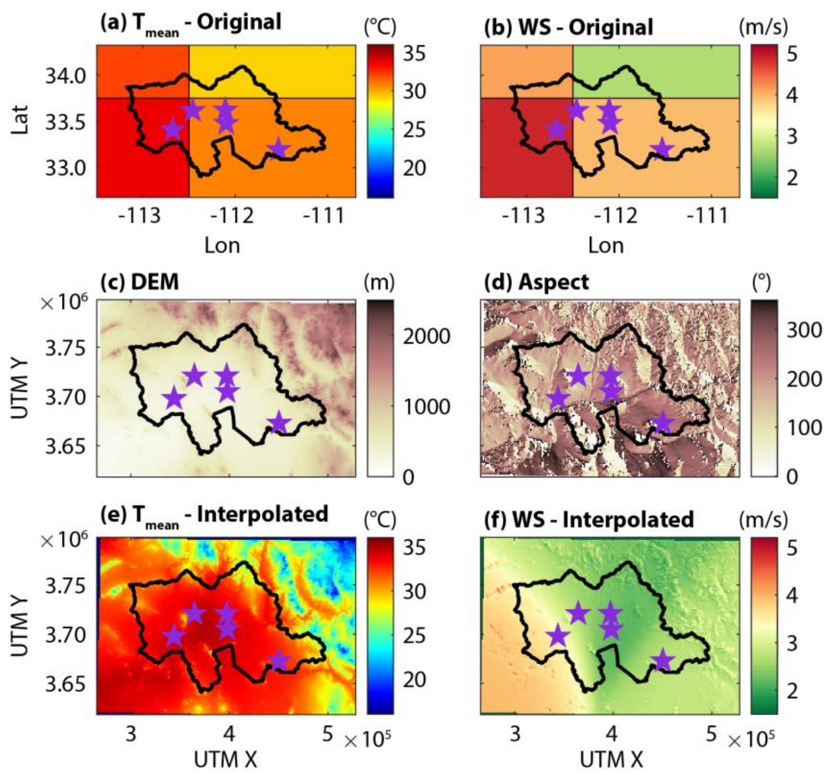

Figure 8. Example of spatial interpolation of T_{mean} and WS for ACCESS-CM2 on 07/31/2014. (a)-(b) Original climate model simulations. (c)-(d) 500-m digital elevation model (DEM) and derived aspect, respectively. (e)-(f) Bias-corrected and spatially interpolated variables. The black line is the boundary of the Phoenix AMA, while the stars are the AZMET weather stations used for the spatial interpolation.

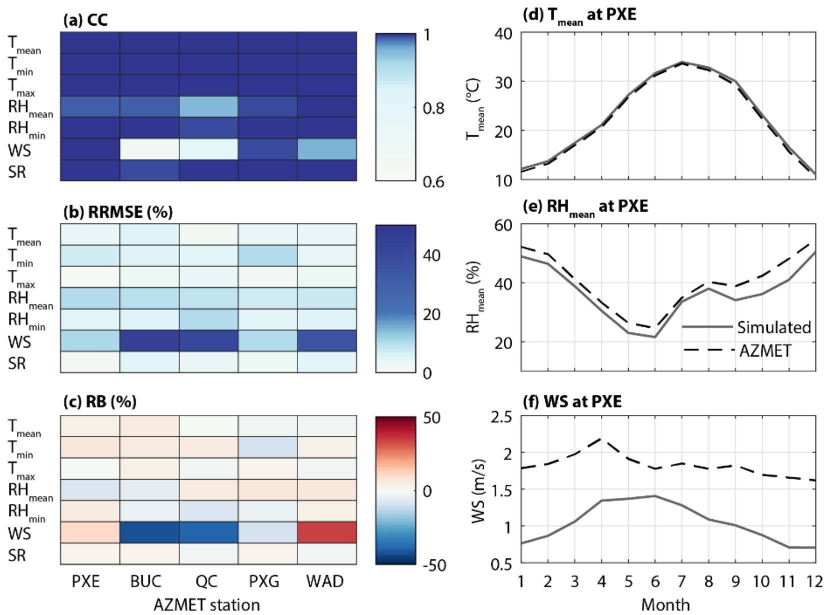

Figure 9. Heat maps of (a) CC, (b) RRMSE, and (c) RB quantifying the ability to simulate the monthly climatology of all variables except P under the leave-one-out cross validation (left out station showing on *x*-axis) of the spatial interpolation method of Liston and Elder (2006). (d)-(f) Climatological monthly means simulated in the leave-one-out verification and observed at the left-out station for selected variables and stations.

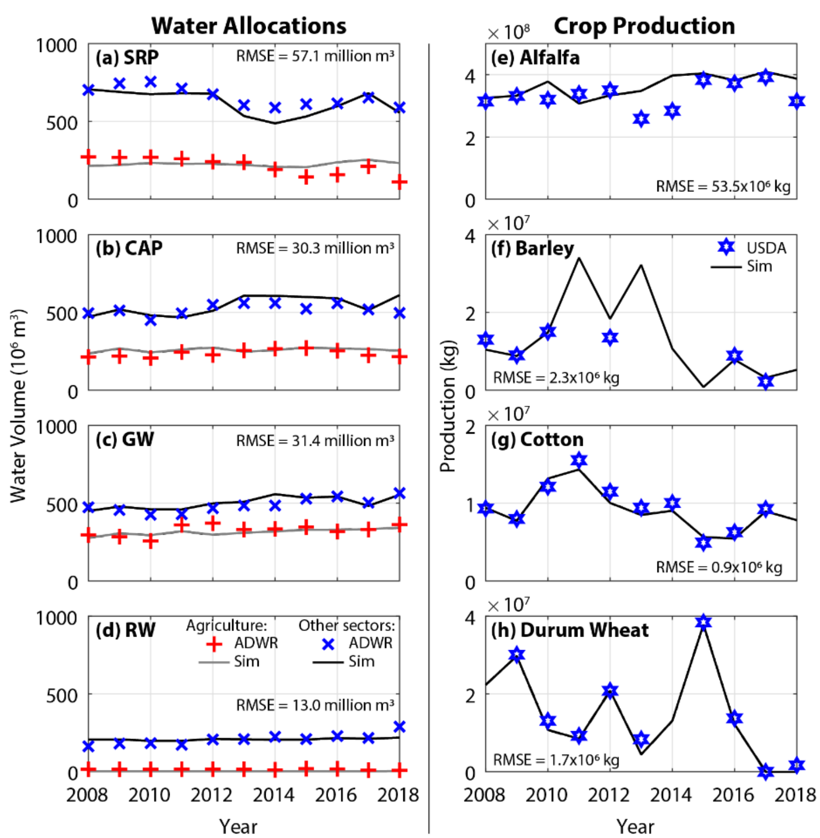

Figure 10. Performance of the calibrated WEAP-MABIA model with the full network and observed climate forcings. (a)-(d) Simulations and estimates from ADWR of annual water allocations from SRP, CAP, groundwater (GW) and reclaimed water (RW) to agricultural and all other demand sectors

(municipal, industrial, power plant and Native American). (e)-(h) Simulations and estimates from USDA of productions of alfalfa hay, barley, cotton, and durum wheat.

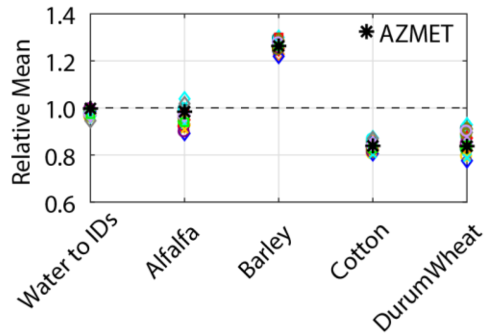

Figure 11. Performance of the calibrated WEAP-MABIA model with the simplified network and forcings from bias corrected GCM outputs in the historical period (legend reported in Fig. 5). Performances are evaluated via the ratio between climatological means of simulations with forcings from each GCM and estimates from ADWR (USDA) for annual water allocations to the IDs (production of alfalfa hay, barley, cotton, and durum wheat). To investigate the effect of variable cultivated area, simulations with the simplified network were also performed under observed forcings at the AZMET stations.

atmospheric humidity content, and cloud radiative forcing (Ruosteenoja et al., 2019; Wild et al., 2015). Finally, the annual ET_{ref} is projected to increase by 125 mm (210 mm) for RCP45 and SSP245 (RCP85 and SSP585) scenarios. This rise is largely driven by increasing temperature, while changes of ET_{ref} due to variations of other climate variables play a minor role.

Fig. 13 summarizes changes in crop production simulated with the simplified WEAP-MABIA network configuration of Fig. 4b under the assumption of no water shortage. The production of all 11 crops combined is projected to decrease differently in the two scenarios (Figs. 13a,b). Under moderate warming, the rate of decrease is higher up to 2060 and reduced afterwards. Differences between the declining rates before and after 2060 are larger for RCP45 than SSP245, as shown in Fig. 13c for each crop. Conversely, under both intense warming scenarios, the decline rate is relatively constant throughout the simulation period (from -4.8 to -1.3%) and higher by ~2% per decade compared to results before 2060 in the moderate warming scenarios. The uncertainty of the projections increases with time and is larger for the intense warming scenarios. Changes in crop production under the irrigation water shortages of the Colorado River Drought Contingency Plan (USBR, 2021) are presented in Fig. 14. The water cuts for the IDs in the Phoenix AMA were estimated by linearly scaling the total volumes prescribed for Arizona under five tiers. WEAP-MABIA was then applied with the simplified network under each tier using climate forcings from the MPI-ESM1-2-HR GCM, whose outputs are closer to the ensemble mean. The reduction due solely to climate change is more than doubled in tier 0 and keeps increasing in a linear fashion at a rate of about -1.8% every 1% of water shortage.

6. Discussion

6.1 Performance of CMIP5 and CMIP6 models

Our analyses assessed the ability of CMIP5 and CMIP6 GCMs to simulate climate variables needed to apply crop models in the desert southwestern U.S. As such, this work complements previous studies focused on P and temperature simulated by CMIP5 models in large domains of U.S. (Sheffield et al., 2013), including southwestern U.S. (Langford et al., 2014) and the Colorado River basin (Gautam and Mascaro, 2018). Furthermore, it provides one of the first assessments of CMIP6 models historical simulations in the region. We found that GCMs simulate quite well the seasonality of temperature but are negatively biased (up to -9.6 ºC; Fig. 6). This finding is in disagreement with Sheffield et al. (2013) who reported a small positive mean bias of nearly +2 ºC in the larger West North American domain, but it is consistent with Gautam and Mascaro (2018) who focused on the lower Colorado River basin that includes our study region. This suggests that the choice of climate models for local impact studies should be based on comparisons at smaller scales. Consistent with prior studies, we found that most GCMs poorly represent the seasonality of P due to the simulation of a delayed and drier NAM season, while winter P is overestimated (Flato et al., 2013). To our knowledge, no study has evaluated performance of historical simulations of the other variables analyzed here in southwestern U.S.

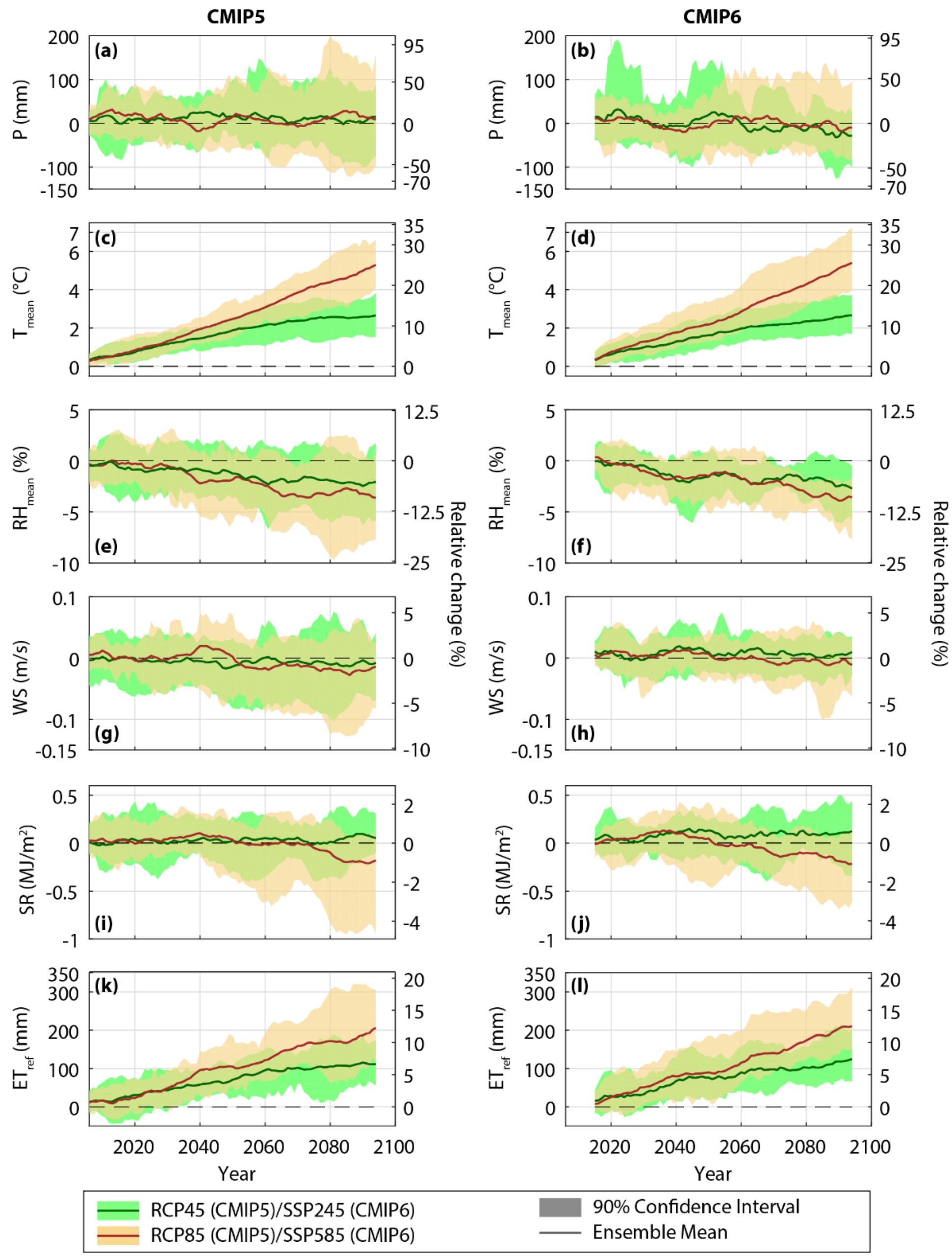

Figure 12. Ensemble mean and 90% CI across CMIP5 and CMIP6 GCMs of the 11-year moving average of the anomalies of P, T_{mean}, RH_{mean}, WS, and SR, and ET_{ref}, spatially averaged in the Phoenix AMA. In each panel, the left axis shows the variable units and the right axis the relative change from the historical mean.

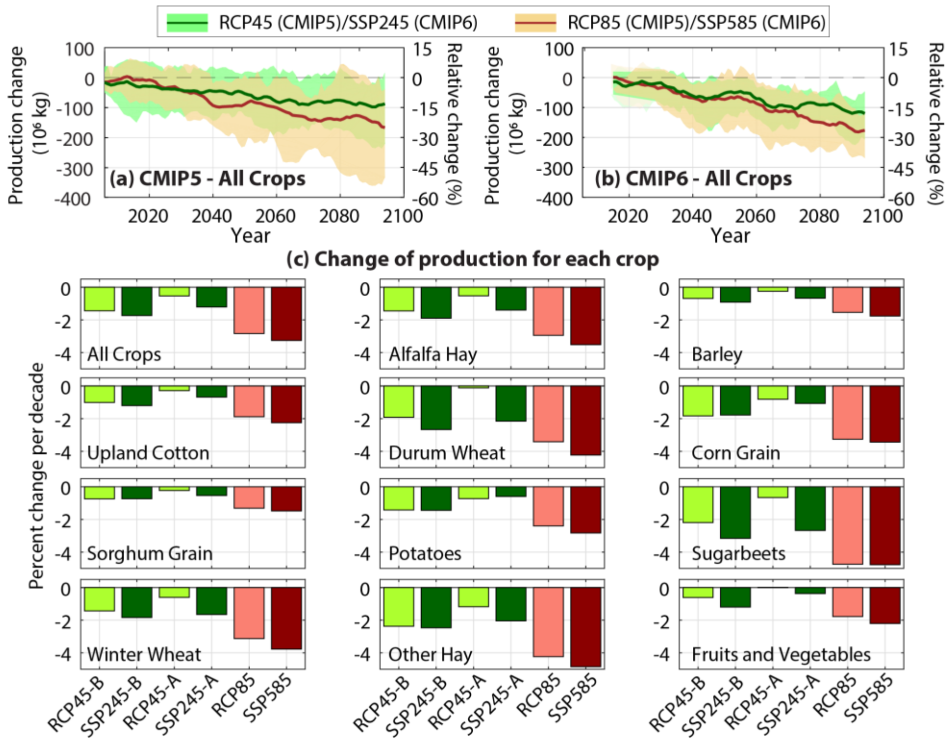

Figure 13. (a)-(b) Ensemble mean and 90% CI across simulations forced with CMIP5 and CMIP6 GCMs of change in production from the historic observed mean of all 11 crops combined. (c) Rate of production change (in % per decade) for all crops assuming linear variability. For the RCP45 than SSP245 scenarios, the rate is reported for the time periods before and after 2060 (labeled B and A, respectively).

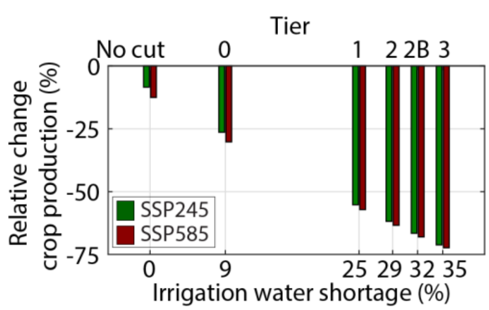

Figure 14. Change in crop production of all 11 crops over the entire simulation period under water shortages estimated from tiers 0, 1, 2, 2B, and 3 of the Colorado River drought contingency plan (USBR, 2021). Simulations have been conducted with forcings from MPI-ESM1-2-HR of CMIP6.

To support impact studies in the study region and compare performance of CMIP5 and CMIP6 models, we ranked the GCMs based on a relative error metric quantifying the ability to simulate the climatology of given variables and all variables combined. Results are reported in Fig. 15 that shows that a large variability in performance exists in terms of which variable is targeted and, to a lower extent, which station is used as reference. For example, CanESM2 (IPSL-CM5A-MR) is the best for P (T_{mean} and RH_{mean}) across all stations, while the ACCESS models simulate well WS. MIROC5 performs remarkably well for all variables and sites, followed by models from INM and CNRM-CM5. On the other hand, the MRI GCMs are the least accurate. The error metrics also reveal that there are no significant differences in performance among GCMs of CMIP5 and CMIP6. This result is likely region-dependent, because studies in Asian regions found CMIP6 models to be more accurate in the simulation of P and temperature (Lun et al., 2021; Zamani et al., 2020) and WS (Krishnan and Bhaskaran, 2020).

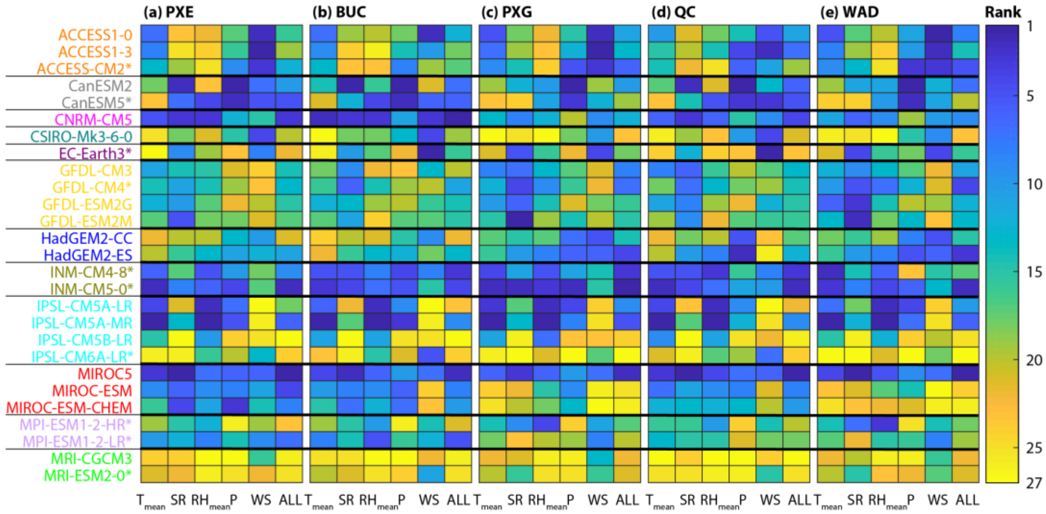

Figure 15. Rank of the relative error defined in Deidda et al. (2013) combining STD, CRMSD, and CC computed for selected climate variables and all climate variables combined using each of the five AZMET stations as reference. GCMs from CMIP6 are marked with an asterisk.

6.2 Controls on changes in crop production

Our simulations suggest that, if no water cut will occur, climate change will lead to a decrease in production ranging, on average, from no variation to -4.8% per decade depending on crop type and climate scenario (Fig. 13c). While the uncertainty across the simulations increases with time, the negative trend is significant and the probability of experiencing increases in production is quite low (Figs. 13a,b). Since GCMs do not simulate substantial variations of annual P, changes in crop production are largely controlled by variations of ET_{ref} and, in turn, of temperature, as it could be visually inferred by comparing the trends in Figs. 13a,b with those in Figs. 12c,d and 12k,l. Under moderate global warming, increases in temperature are projected to slow down in 2060, thus explaining the lower reductions in crop production simulated after this year (Fig. 13). If warming will be intense, crop production will instead decrease over the next century with a nearly linear rate of -5.0% per 1 ºC averaged across all crops and scenarios. The effect of climate change will become relatively less important if water shortages will occur, as revealed in Fig. 14 by the rates of decrease of the two emission scenarios becoming similar after tier 1. In other words, the intensity of global warming will not significantly affect reductions in crop production once water cuts will exceed 10% of current allocations.

Differences in production changes across crops (Fig. 13c) are mainly controlled by the value of the basal crop coefficient (K_{cb}), which is used in MABIA in the computation of actual evapotranspiration (ET_a) from ET_{ref} (see Section 4.1.1 and Supplementary Material). Crops with larger K_{cb} (e.g., other hay) tend to have higher ET_a and, in turn, experience more severe water deficits under the same available water for irrigation. Since yield is linearly related with water deficit, crops with higher K_{cb} face higher reductions in yield and, then, productivity.

Our estimates of variation in production for distinct crops are largely consistent with existing studies in the region in terms of sign, while they differ in terms of magnitude. Wing et al. (2015) evaluated the production change of major crops in U.S. through an empirical statistical model under different greenhouse gas emission scenarios and found that, in southwestern U.S., production of wheat and cotton is projected to decrease with a constant rate (rate that decreases after 2050s) for a scenario equivalent to RCP85 (RCP45), as found here, although with slightly smaller magnitude. On the other hand, these authors predicted an increase in production of corn. Differences in magnitude with our results can be attributed to the fact that Wing et al. (2015) accounted for the CO_2 fertilization effect in their empirical model, which is not taken into account by MABIA. Berardy and Chester (2017) estimated yield variations for several crops in Arizona under different temperature changes related to climate change.

Consistent with our results, these authors estimated a decrease in production for all crops, but with larger magnitudes. These discrepancies can be explained by the fact that their model accounts for potential interruptions of irrigation due energy shortages, among other causes, while we assumed irrigation water to be constantly available.

7. Conclusions

The main conclusions of this study are as follows:

(1) Simulations of WEAP-MABIA under observed climate forcings capture well historical water allocations from supply sources to all demand sectors and crop production at the ID scale in the Phoenix AMA.

(2) GCM outputs reproduce very well amplitude and phasing of the annual cycle of T_{mean} (SR) although with a mean negative (positive) bias. This capability degrades gradually for RH_{mean}, P, and WS. In particular, GCMs simulate a delayed and drier NAM and wetter winter P. While the relative ability of the GCMs depend on the targeted variable, MIROC5 and models from INM and CNRM-CM5 perform particularly well in this region. No significant differences in performance emerge among GCMs of CMIP5 and CMIP6.

(3) The parametric quantile mapping bias correction method of Mamalakis et al. (2017) was found to perform well for P, the variance scaling of Chen et al. (2011) for temperature, and the nonparametric quantile mapping for all other variables. The combination of these bias correction techniques with a spatial interpolation accounting for terrain properties applied to historical GCM outputs allowed reproducing quite well the historical climatology of all variables at five weather stations. The use of these bias corrected climate forcings as input for WEAP-MABIA, in turn, permitted capturing the observed mean water allocations to the agricultural sector and of crop production in the study region.

(4) In the Phoenix AMA, the ensemble mean of the GCMs projects T_{mean} (RH_{mean}) to increase (decrease) in 2100 by 2.7 ºC and 5.4 ºC (2.7% and 3.6%) for the moderate and intense warming scenarios, respectively. Changes in T_{mean} will lead to a rise in ET_{ref} by 125 mm and 210 mm by the end of the century in the two scenarios. P, WS and SR are not expected to change significantly. For all variables, the uncertainty across the GCMs increases with time.

(5) Changes in climate variables under the assumption of no water shortages will lead to reductions in crop production with rates that, under moderate warming scenarios, are higher up to 2060 and reduced afterwards, while they stay constant through 2100 under intense warming scenarios. The rates of change range, on average, from negligible values for fruits and vegetables to -4.8% per decade for other hay; the declines under intense warming are more significant (~2% higher) and with larger uncertainty compared to those under moderate warming. Changes in crop productivity are largely driven by increases in ET_{ref} and, in turn, of temperature.

(6) As expected, irrigation water shortages will lead to additional, significant reductions in crop production, estimated in -1.8% every 1% of water cuts. The effect of climate change on crop production is expected to become less important if water shortages will exceed 10% of current allocations, which could occur under the recently approved Colorado River Drought Contingency Plan.

References

Adams, D.K., Comrie, A.C., 1997. The North American Monsoon. Bull. Am. Meteorol. Soc. 78, 2197–2213. https://doi.org/10.1175/1520-0477(1997)078<2197:TNAM>2.0.CO;2

ADWR, 2021a. AMA Annual Supply And Demand Data. Arizona Department of Water Resources. URL https://new.azwater.gov/ama/ama-data (accessed 3.8.21).

ADWR, 2021b. Well registry web. Arizona Department of Water Resources. URL http://gisweb.azwater.gov/waterresourcedata/wellregistry.aspx (accessed 3.8.21).

Allen, R.G., Pereira, L.S., Raes, D., Smith, M., 1998. Crop evapotranspiration - Guidelines for computing crop water requirements. FAO Irrigation and drainage paper No. 56, Food and Agriculture

Organization of the United Nations. Rome.
Barnes, S.L., 1994. Applications of the Barnes objective analysis scheme. Part I: effects of undersampling, wave position, and station randomness. J. Atmos. Ocean. Technol. 11, 1433–1479. https://doi.org/10.1175/1520-0426(1994)011<1433:aotboa>2.0.co;2
Bausch, J.C., Eakin, H., Smith-Heisters, S., York, A.M., White, D.D., Rubiños, C., Aggarwal, R.M., 2015. Development pathways at the agriculture–urban interface: the case of Central Arizona. Agric. Human Values 32, 743–759. https://doi.org/10.1007/s10460-015-9589-8
Berardy, A., Chester, M. V, 2017. Climate change vulnerability in the food, energy, and water nexus: concerns for agricultural production in Arizona and its urban export supply. Environ. Res. Lett. 12, 035004. https://doi.org/10.1088/1748-9326/aa5e6d
Boé, J., Terray, L., Habets, F., Martin, E., 2007. Statistical and dynamical downscaling of the Seine basin climate for hydro-meteorological studies. Int. J. Climatol. 27, 1643–1655. https://doi.org/10.1002/joc.1602
Brouwer, C., Prins, K., Heibloem, M., 1989. Irrigation Water Management: Irrigation Scheduling. Training manual no. 4, FAO.
Brown, P., 2005. Standardized reference evapotranspiration: A new procedure for estimating reference evapotranspiration in Arizona. Available at https://extension.arizona.edu/sites/extension.arizona.edu/files/pubs/az1324.pdf
CAP, 2021. CAP water deliveries. Central Arizona Project. URL https://www.cap-az.com/departments/water-operations/deliveries (accessed 4.12.21).
Chen, J., Brissette, F.P., Leconte, R., 2011. Uncertainty of downscaling method in quantifying the impact of climate change on hydrology. J. Hydrol. 401, 190–202. https://doi.org/10.1016/j.jhydrol.2011.02.020
City of Phoenix Water Service Department, 2011. 2011 Water Resource Plan.
Cook, E.R., Seager, R., Cane, M.A., Stahle, D.W., 2007. North American drought: Reconstructions, causes, and consequences. Earth-Science Rev. 81, 93–134. https://doi.org/10.1016/j.earscirev.2006.12.002
Corbeels, M., Berre, D., Rusinamhodzi, L., Lopez-Ridaura, S., 2018. Can we use crop modelling for identifying climate change adaptation options? Agric. For. Meteorol. 256, 46–52.
Deidda, R., Marrocu, M., Caroletti, G., Pusceddu, G., Langousis, A., Lucarini, V., Puliga, M., Speranza, A., 2013. Regional climate models' performance in representing precipitation and temperature over selected Mediterranean areas. Hydrol. Earth Syst. Sci. 17, 5041–5059. https://doi.org/10.5194/hess-17-5041-2013
Doorenbos, J., Kassam, A.H., 1979. Yield response to water. FAO Irrigation and Drainage Paper Number 33, Food and Agriculture Organization of the United Nations. Rome.
Duval, D., Bickel, A.K., Frisvold, G., Wu, X., Hu, C., 2018. Contribution of agriculture to the Maricopa County and Gila River Indian community economies, Department of Agricultural and Resource Economics, Cooperative Extension, The University of Arizona.
Easterling, D.R., Arnold, J., Knutson, T., Kunkel, K., LeGrande, A., Leung, L.R., Vose, R., Waliser, D., Wehner, M., 2017. Precipitation change in the United States, Climate Science Special Report: Fourth National Climate Assessment, Volume I. Washington, DC.
Elias, E., Rango, A., Smith, R., Maxwell, C., Steele, C., Havstad, K., 2016. Climate Change, Agriculture and Water Resources in the Southwestern United States. J. Contemp. Water Res. Educ. 158, 46–61. https://doi.org/10.1111/j.1936-704x.2016.03218.x
Esteve, P., Varela-Ortega, C., Blanco-Gutiérrez, I., Downing, T.E., 2015. A hydro-economic model for the assessment of climate change impacts and adaptation in irrigated agriculture. Ecol. Econ. 120, 49–58. https://doi.org/10.1016/j.ecolecon.2015.09.017
Fan, C., Myint, S.W., Rey, S.J., Li, W., 2017. Time series evaluation of landscape dynamics using annual Landsat imagery and spatial statistical modeling: evidence from the Phoenix metropolitan region. Int. J. Appl. Earth Obs. Geoinf. 58, 12–25. https://doi.org/10.1016/j.jag.2017.01.009
Fawcett, P.J., Werne, J.P., Anderson, R.S., Heikoop, J.M., Brown, E.T., Berke, M.A., Smith, S.J., Goff,

F., Donohoo-Hurley, L., Cisneros-Dozal, L.M., 2011. Extended megadroughts in the southwestern United States during Pleistocene interglacials. Nature 470, 518–521. https://doi.org/10.1038/nature09839
Flato, G., Marotzke, J., Abiodun, B., Braconnot, P., Chou, S.C., Collins, W., Cox, P., Driouech, F., Emori, S., Eyring, V., 2013. Evaluation of climate models, in: Climate Change 2013 the Physical Science Basis: Working Group I Contribution to the Fifth Assessment Report of the Intergovernmental Panel on Climate Change. Cambridge University Press, pp. 741–866. https://doi.org/10.1017/CBO9781107415324.020
Fraga, H., Pinto, J.G., Viola, F., Santos, J.A., 2020. Climate change projections for olive yields in the Mediterranean Basin. Int. J. Climatol. 40, 769–781.
French, A.N., Hunsaker, D.J., Bounoua, L., Karnieli, A., Luckett, W.E., Strand, R., 2018. Remote sensing of evapotranspiration over the central Arizona irrigation and drainage district, USA. Agronomy 8, 278. https://doi.org/10.3390/agronomy8120278
Gautam, J., Mascaro, G., 2018. Evaluation of Coupled Model Intercomparison Project Phase 5 historical simulations in the Colorado River basin. Int. J. Climatol. 38, 3861–3877. https://doi.org/10.1002/joc.5540
Guan, X., Mascaro, G., Sampson, D., Maciejewski, R., 2020. A metropolitan scale water management analysis of the food-energy-water nexus. Sci. Total Environ. 701, 134478. https://doi.org/10.1016/j.scitotenv.2019.134478
Higdon, P.H., Thompson, T.W., 1980. The 1980 Arizona Groundwater Management Code. Ariz. St. L.J. 621.
Jabloun, M., Sahli, A., 2012. WEAP-MABIA tutorial: A collection of stand-alone chapters to aid in learning the WEAP-MABIA module.
Jones, J.L., White, D.D., 2021. A social network analysis of collaborative governance for the food-energy-water nexus in Phoenix, AZ, USA. J. Environ. Stud. Sci. 1–11. https://doi.org/10.1007/s13412-021-00676-3
Jones, J.W., Hoogenboom, G., Porter, C.H., Boote, K.J., Batchelor, W.D., Hunt, L.A., Wilkens, P.W., Singh, U., Gijsman, A.J., Ritchie, J.T., 2003. The DSSAT cropping system model. Eur. J. Agron. 18, 235–265. https://doi.org/10.1016/S1161-0301(02)00107-7
Keating, B.A., Carberry, P.S., Hammer, G.L., Probert, M.E., Robertson, M.J., Holzworth, D., Huth, N.I., Hargreaves, J.N.G., Meinke, H., Hochman, Z., McLean, G., Verburg, K., Snow, V., Dimes, J.P., Silburn, M., Wang, E., Brown, S., Bristow, K.L., Asseng, S., Chapman, S., McCown, R.L., Freebairn, D.M., Smith, C.J., 2003. An overview of APSIM, a model designed for farming systems simulation. Eur. J. Agron. 18, 267–288. https://doi.org/10.1016/S1161-0301(02)00108-9
Koch, S.E., Desjardins, M., Kocin, P.J., 1983. An interactive Barnes objective map analysis scheme for use with satellite and conventional data. J. Clim. Appl. Meteorol. 22, 1487–1503. https://doi.org/10.1175/1520-0450(1983)022<1487:AIBOMA>2.0.CO;2
Kolankiewicz, L., Beck, R., Ruark, E.A., 2020. Population Growth and the Diminishing Natural State of Arizona. Analysis of National Resources Inventory & U.S. Census Data on Development and Habitat Loss in a Thirsty Grand Canyon State. Available at https://www.numbersusa.org/sites/default/files/public/2020_AZ_Sprawl_Study.pdf
Krishnan, A., Bhaskaran, P.K., 2020. Skill assessment of global climate model wind speed from CMIP5 and CMIP6 and evaluation of projections for the Bay of Bengal. Clim. Dyn. 55, 2667–2687. https://doi.org/10.1007/s00382-020-05406-z
Langford, S., Stevenson, S., Noone, D., 2014. Analysis of low-frequency precipitation variability in CMIP5 historical simulations for southwestern North America. J. Clim. 27, 2735–2756. https://doi.org/10.1175/JCLI-D-13-00317.1
Laux, P., Rötter, R.P., Webber, H., Dieng, D., Rahimi, J., Wei, J., Faye, B., Srivastava, A.K., Bliefernicht, J., Adeyeri, O., Arnault, J., Kunstmann, H., 2021. To bias correct or not to bias correct? An agricultural impact modelers' perspective on regional climate model data. Agric. For. Meteorol. 304–305, 108406. https://doi.org/10.1016/j.agrformet.2021.108406

Leck, H., Conway, D., Bradshaw, M., Rees, J., 2015. Tracing the water-energy-food nexus: description, theory and practice. Geogr. Compass 9, 445–460. https://doi.org/10.1111/gec3.12222

Liston, G.E., Elder, K., 2006. A meteorological distribution system for high-resolution terrestrial modeling (MicroMet). J. Hydrometeorol. 7, 217–234.

Lun, Y., Liu, L., Cheng, L., Li, X., Li, H., Xu, Z., 2021. Assessment of GCMs simulation performance for precipitation and temperature from CMIP5 to CMIP6 over the Tibetan Plateau. Int. J. Climatol. https://doi.org/10.1002/joc.7055

MacDonald, G.M., 2010. Water, climate change, and sustainability in the southwest. Proc. Natl. Acad. Sci. 107, 21256–21262. https://doi.org/10.1073/pnas.0909651107

MacDonald, G.M., Stahle, D.W., Villanueva Diaz, J., Beer, N., Busby, S.J., Cerano-Paredes, J., Cole, J.E., Cook, E.R., End-Field, G., Gutierrez-Garcia, G., Hall, B., Magana, V., Meko, D.M., Méndez-Pérez, M., Sauchyn, D.J., Watson, E., Woodhouse, C.A., 2008. Climate warming and 21st-century drought in southwestern North America. Eos (Washington. DC). 89, 82. https://doi.org/10.1029/2008EO090003

MAG, 2021. The Phoenix Metropolitan Statistical Area Population. Maricopa Association of Governments. URL https://www.azmag.gov/Programs/Maps-and-Data/Community-Profiles (accessed 3.8.21).

Mamalakis, A., Langousis, A., Deidda, R., Marrocu, M., 2017. A parametric approach for simultaneous bias correction and high-resolution downscaling of climate model rainfall. Water Resour. Res. 53, 2149–2170. https://doi.org/10.1002/2016WR019578

Mascaro, G., 2017. Multiscale spatial and temporal statistical properties of rainfall in central Arizona. J. Hydrometeorol. 18, 227–245. https://doi.org/10.1175/JHM-D-16-0167.1

Mounir, A., Guan, X., Mascaro, G., 2021. Quantifying the value of spatiotemporal resolutions and feedback loops in water-energy nexus modeling. Unpublished results. Under review in Environmental Modelling & Software.

Mounir, A., Mascaro, G., White, D.D., 2019. A metropolitan scale analysis of the impacts of future electricity mix alternatives on the water-energy nexus. Appl. Energy 256, 113870. https://doi.org/10.1016/j.apenergy.2019.113870

Müller, C., Franke, J., Jägermeyr, J., Ruane, A.C., Elliott, J., Moyer, E., Heinke, J., Falloon, P.D., Folberth, C., Francois, L., Hank, T., Izaurralde, R.C., Jacquemin, I., Liu, W., Olin, S., Pugh, T.A.M., Williams, K., Zabel, F., 2021. Exploring uncertainties in global crop yield projections in a large ensemble of crop models and CMIP5 and CMIP6 climate scenarios. Environ. Res. Lett. 16, 34040. https://doi.org/10.1088/1748-9326/abd8fc

O'Gorman, P.A., Muller, C.J., 2010. How closely do changes in surface and column water vapor follow Clausius-Clapeyron scaling in climate change simulations? Environ. Res. Lett. 5, 25207. https://doi.org/10.1088/1748-9326/5/2/025207

O'Neill, B.C., Tebaldi, C., Van Vuuren, D.P., Eyring, V., Friedlingstein, P., Hurtt, G., Knutti, R., Kriegler, E., Lamarque, J.F., Lowe, J., Meehl, G.A., Moss, R., Riahi, K., Sanderson, B.M., 2016. The Scenario Model Intercomparison Project (ScenarioMIP) for CMIP6. Geosci. Model Dev. 9, 3461–3482. https://doi.org/10.5194/gmd-9-3461-2016

Osborne, T., Rose, G., Wheeler, T., 2013. Variation in the global-scale impacts of climate change on crop productivity due to climate model uncertainty and adaptation. Agric. For. Meteorol. 170, 183–194.

Peng, B., Guan, K., Tang, J., Ainsworth, E.A., Asseng, S., Bernacchi, C.J., Cooper, M., Delucia, E.H., Elliott, J.W., Ewert, F., Grant, R.F., Gustafson, D.I., Hammer, G.L., Jin, Z., Jones, J.W., Kimm, H., Lawrence, D.M., Li, Y., Lombardozzi, D.L., Marshall-Colon, A., Messina, C.D., Ort, D.R., Schnable, J.C., Vallejos, C.E., Wu, A., Yin, X., Zhou, W., 2020. Towards a multiscale crop modelling framework for climate change adaptation assessment. Nat. Plants 6, 338–348. https://doi.org/10.1038/s41477-020-0625-3

Phillips, D.H., Reinink, Y., Skarupa, T.E., Ester, C.E., Skindlov, J.A., 2009. Water resources planning and management at the Salt River Project, Arizona, USA. Irrig. Drain. Syst. 23, 109. https://doi.org/10.1007/s10795-009-9063-0

Reidmiller, D.R., Avery, C.W., Easterling, D.R., Kunkel, K.E., Lewis, K.L.M., Maycock, T.K., Stewart, B.C., 2018. Impacts, risks, and adaptation in the United States: Fourth national climate assessment, volume II. Washington, DC, USA. https://doi.org/10.7930/NCA4.2018
Ringler, C., Bhaduri, A., Lawford, R., 2013. The nexus across water, energy, land and food (WELF): potential for improved resource use efficiency? Curr. Opin. Environ. Sustain. 5, 617–624. https://doi.org/10.1016/j.cosust.2013.11.002
Ruosteenoja, K., Räisänen, P., Devraj, S., Garud, S.S., Lindfors, A. V., 2019. Future changes in incident surface solar radiation and contributing factors in India in CMIP5 climate model simulations. J. Appl. Meteorol. Climatol. 58, 19–35. https://doi.org/10.1175/JAMC-D-18-0013.1
Sanderson, B.M., Wehner, M., Knutti, R., 2017. Skill and independence weighting for multi-model assessments. Geosci. Model Dev. 10, 2379–2395. https://doi.org/10.5194/gmd-10-2379-2017
Schlenker, W., Roberts, M.J., 2009. Nonlinear temperature effects indicate severe damages to US crop yields under climate change. Proc. Natl. Acad. Sci. 106, 15594–15598.
Seager, R., Ting, M., Held, I., Kushnir, Y., Lu, J., Vecchi, G., Huang, H.-P., Harnik, N., Leetmaa, A., Lau, N.-C., 2007. Model projections of an imminent transition to a more arid climate in southwestern North America. Science (80-.). 316, 1181–1184. https://doi.org/10.1126/science.1139601
Sheffield, J., Barrett, A.P., Colle, B., Fernando, D.N., Fu, R., Geil, K.L., Hu, Q., Kinter, J., Kumar, S., Langenbrunner, B., Lombardo, K., Long, L.N., Maloney, E., Mariotti, A., Meyerson, J.E., Mo, K.C., Neelin, J.D., Nigam, S., Pan, Z., Ren, T., Ruiz-Barradas, A., Serra, Y.L., Seth, A., Thibeault, J.M., Stroeve, J.C., Yang, Z., Yin, L., 2013. North American Climate in CMIP5 experiments. Part I: Evaluation of historical simulations of continental and regional climatology. J. Clim. 26, 9209–9245. https://doi.org/10.1175/JCLI-D-12-00592.1
Sheppard, P.R., Comrie, A.C., Packin, G.D., Angersbach, K., Hughes, M.K., 2002. The climate of the US Southwest. Clim. Res. 21, 219–238. https://doi.org/10.3354/cr021219
Sherwood, S., Fu, Q., 2014. A drier future? Science (80-.). 343, 737–739. https://doi.org/10.1126/science.1247620
Simmons, A.J., Willett, K.M., Jones, P.D., Thorne, P.W., Dee, D.P., 2010. Low-frequency variations in surface atmospheric humidity, temperature, and precipitation: Inferences from reanalyses and monthly gridded observational data sets. J. Geophys. Res. Atmos. 115. https://doi.org/10.1029/2009JD012442
Sommer, R., Glazirina, M., Yuldashev, T., Otarov, A., Ibraeva, M., Martynova, L., Bekenov, M., Kholov, B., Ibragimov, N., Kobilov, R., 2013. Impact of climate change on wheat productivity in Central Asia. Agric. Ecosyst. Environ. 178, 78–99.
SRP, 2021. Watershed connection. Salt River Project. URL https://streamflow.watershedconnection.com/Dwr (accessed 4.12.21).
Steele, C., Reyes, J., Elias, E., Aney, S., Rango, A., 2018. Cascading impacts of climate change on southwestern US cropland agriculture. Clim. Change 148, 437–450.
Taylor, K.E., 2001. Summarizing multiple aspects of model performance in a single diagram. J. Geophys. Res. Atmos. 106, 7183–7192. https://doi.org/10.1029/2000JD900719
Teutschbein, C., Seibert, J., 2012. Bias correction of regional climate model simulations for hydrological climate-change impact studies: Review and evaluation of different methods. J. Hydrol. 456, 12–29. https://doi.org/10.1016/j.jhydrol.2012.05.052
Tubiello, F.N., Rosenzweig, C., Goldberg, R.A., Jagtap, S., Jones, J.W., 2002. Effects of climate change on US crop production: simulation results using two different GCM scenarios. Part I: wheat, potato, maize, and citrus. Clim. Res. 20, 259–270. https://doi.org/10.3354/cr020259
Udall, B., Overpeck, J., 2017. The twenty-first century Colorado River hot drought and implications for the future. Water Resour. Res. 53, 2404–2418. https://doi.org/10.1002/2016WR019638
USBR, 2021. Colorado River Basin Drought Contingency Plans. Bureau of Reclamation. URL https://www.usbr.gov/dcp/finaldocs.html (accessed 4.8.21).
USDA, 2021a. Quick Stats. U.S. Department of Agriculture, National Agricultural Statistics Service.

URL https://quickstats.nass.usda.gov/ (accessed 4.22.21).
USDA, 2021b. 2017 Census of Agriculture, County Profile, Maricopa County, Arizona. U.S. Department of Agriculture, National Agricultural Statistics Service. URL https://www.nass.usda.gov/Publications/AgCensus/2017/Online_Resources/County_Profiles/Arizona/cp04013.pdf (accessed 3.11.21).
USDA, 2021c. CropScape and Cropland Data Layer. U.S. Department of Agriculture, National Agricultural Statistics Service. URL https://www.nass.usda.gov/Research_and_Science/Cropland/Release/ (accessed 3.11.21).
USDA, 2021d. Web Soil Survey. U.S. Department of Agriculture, Natural Resources Conservation Service. URL https://websoilsurvey.sc.egov.usda.gov/App/WebSoilSurvey.aspx (accessed 4.12.21).
USGS, 2021. 3D Elevation Program (3DEP). U.S. Geological Survey. URL https://www.usgs.gov/core-science-systems/ngp/3dep/about-3dep-products-services?qt-science_support_page_related_con=0#qt-science_support_page_related_con (accessed 4.22.21).
van Vuuren, D.P., Edmonds, J., Kainuma, M., Riahi, K., Thomson, A., Hibbard, K., Hurtt, G.C., Kram, T., Krey, V., Lamarque, J.F., Masui, T., Meinshausen, M., Nakicenovic, N., Smith, S.J., Rose, S.K., 2011. The representative concentration pathways: An overview. Clim. Change 109, 5–31. https://doi.org/10.1007/s10584-011-0148-z
Vose, R., Easterling, D.R., Kunkel, K., Wehner, M., 2017. Temperature changes in the United States, Climate Science Special Report: Fourth National Climate Assessment, Volume I. Washington, DC, USA. https://doi.org/10.7930/J0N29V45
Wang, Xiaowen, Li, L., Ding, Y., Xu, J., Wang, Y., Zhu, Y., Wang, Xiaoyun, Cai, H., 2021. Adaptation of winter wheat varieties and irrigation patterns under future climate change conditions in Northern China. Agric. Water Manag. 243, 106409. https://doi.org/10.1016/j.agwat.2020.106409
WEAP, 2020. MABIA Method. URL https://www.weap21.org/WebHelp/Mabia_Algorithms.htm (accessed 4.21.21).
White, J.W., Hoogenboom, G., Kimball, B.A., Wall, G.W., 2011. Methodologies for simulating impacts of climate change on crop production. F. Crop. Res. 124, 357–368. https://doi.org/10.1016/j.fcr.2011.07.001
Wild, M., Folini, D., Henschel, F., Fischer, N., Müller, B., 2015. Projections of long-term changes in solar radiation based on CMIP5 climate models and their influence on energy yields of photovoltaic systems. Sol. Energy 116, 12–24. https://doi.org/10.1016/j.solener.2015.03.039
Wing, I.S., Monier, E., Stern, A., Mundra, A., 2015. US major crops' uncertain climate change risks and greenhouse gas mitigation benefits. Environ. Res. Lett. 10, 115002.
Yates, D., Averyt, K., Flores-Lopez, F., Meldrum, J., Sattler, S., Sieber, J., Young, C., 2013. A water resources model to explore the implications of energy alternatives in the southwestern US. Environ. Res. Lett. 8, 045004. https://doi.org/10.1088/1748-9326/8/4/045004
Yates, D., Sieber, J., Purkey, D., Huber-Lee, A., 2005. WEAP21 - A demand-, priority-, and preference-driven water planning model. Part 1: model characteristics. Water Int. 30, 487–500. https://doi.org/10.1080/02508060508691893
Zamani, Y., Monfared, S.A.H., Hamidianpour, M., 2020. A comparison of CMIP6 and CMIP5 projections for precipitation to observational data: the case of Northeastern Iran. Theor. Appl. Climatol. 142, 1613–1623.